POD ANALYSIS AND PREDICTION OF CAVITY FLOW INSTABILITY

Edward J. Brooksbank, Aldo Rona
Department of Engineering, University of Leicester, Leicester, LE1 7RH, UK
Email: ejb13@leicester.ac.uk

Abstract

Aircraft with internal store bays are subject to large amplitude pressure oscillations that, at certain flow conditions, may damage both the bay and the stores. To control these oscillations, a method is required to predict in real-time the store bay flow conditions and use these predictions as feed-back to a control device. This study addresses the design of such a flow predictor, based on a Proper Orthogonal Decomposition (POD) approach.

A time dependent numerical model has been developed to investigate the instability of a Mach 1.5 cavity flow. The numerically generated flow history is analysed through the use of POD. Using the methods of snapshots, the large-scale features of the cavity flow can be captured in only a few eigenmodes. A novel method is presented whereby the flow can be accurately predicted, beyond the initial flow history, by decomposing the coefficients applied to the eigenmodes into a short discrete Fourier series.

Results are presented for the flow state predicted 10 fundamental instability mode periods beyond the end of the initial flow history. The method is shown to be very effective and predicted pressures at the downstream edge of the cavity are in excellent agreement with a comparative CFD computation. The accuracy of the prediction is shown to be dependent on the number of snapshots taken for the POD analysis. When a small non-optimal number of snapshots is used, the pressure fluctuation amplitude is not adequately predicted. Even so, the error in phase is small and the general structure of the pressure trace is still captured, making the current method a good candidate for active flow control.

INTRODUCTION

Large amplitude flow instabilities commonly affect the compressible flow in and around a rectangular enclosure. The unsteady flow in the enclosure, or cavity, is characterised by

large amplitude pressure oscillations, an unsteady vorticity field, and flow recirculation in the enclosure (Fig. 1). This leads to a sustained aerodynamic loading, pressure drag, and noise. In an 'open' cavity,[1] the flow instability is driven by the fluctuations of a shear layer that spans across the enclosure.[2] The interaction of the shear layer with the rear bulkhead is part of a feed-back loop which self-sustains the instability.

Cavity flows are an established interest of the academic community.[3,4,5] Numerical, analytical, and experimental models have been developed to investigate the essential physics of the cavity flow instability and to assess suppression methods. An overview of past work is given in Grace.[6] Research work initiated at Cambridge[7] and then continued at the University of Southampton[2,8,9] highlighted the use of time-dependent two-dimensional numerical models to reproduce the large-scale convecting instabilities that characterise the unsteady shear layer over the cavity opening.

The use of active controllers to suppress the cavity flow instability and minimise pressure fluctuations requires the implementation of control devices. In order to design an implementable feed-back controller to drive these devices, it is necessary to have a low order real-time control algorithm that is computationally efficient. Such a controller requires a flow predictor as input to the system.

The POD method,[10] also known as principal component analysis or Karhunen-Loève expansion, is a technique used to capture the overall behaviour of a dynamic system and is used in the current study as a flow predictor. The method generates an eigenvector matrix that captures the non-linearity of the input system with the advantages that the eigenvector elements are ordered from the first element with the highest average energy to the element with the lowest average energy. This is an optimal basis from which to reconstruct the flow, as the first elements contain most of the energy of the flow. In this approach, a desired energy level can be specified and only those eigenvectors or basis elements needed to achieve such a level are stored to project the flow prediction in time.

FLOW CONDITIONS AND NUMERICAL MODEL

A rectangular enclosure is tested at transonic flow conditions, as shown diagrammatically in Fig. 1. The cavity length to depth ratio is 3 and the inlet flow Mach number is 1.5. The geometry and inflow parameters are designed to match the experimental conditions of a selected test in Zhang.[7] At these conditions, the flow develops large amplitude fluctuations and the unsteady shear layer re-attaches on the downstream edge, giving an 'open' cavity regime.[1] A turbulent boundary layer develops above the upstream cavity edge. All dimensions are normalised by the 15mm cavity depth D. At the computational domain inlet boundary b1, the boundary layer thickness δ_{99} is $0.333D$. Above the boundary layer, the uniform free stream speed U_∞, Mach number M_∞, density ρ_∞, static pressure p_∞, and static temperature T_∞ are 425.2m/s, 1.5, 0.9373kg/m^3, 53.801kN/m^2, and 200K respectively. All cavity flow results are normalised by the above free stream values and D/U_∞ normalises time.

The shear layer is characterised by a coupled motion of shear layer flapping in the transverse direction, due to the shear layer instability, and of vortex convection in the streamwise direction, with vortices impinging on the rear bulkhead. The interaction of

the shear layer with the cavity downstream edge establishes a feed-back loop resulting in a self-sustained stationary flow oscillation in the cavity. A detailed description of the cavity flow dynamics is given in Rona & Brooksbank[3] and in the references therein.

The numerical method that is being used is an extension of the scheme by Rona & Dieudonné,[11] where a laminar cavity model at a similar flow regime was presented. The extended finite volume method is based on the discrete time-dependent Reynolds averaged Navier-Stokes equations with k-ω turbulence closure, including ω cross-diffusion.[12] Details are reported in Rona & Bennett[13] and in Rona & Brooksbank.[3]

PROPER ORTHOGONAL DECOMPOSITION

A method is presented whereby the data required to predict the unsteady flow in the cavity at a given time $t > t_0$ can be generated from a Proper Orthogonal Decomposition of a finite cavity flow history $0 < t < t_0$. In the current study, the pressure field has been used to determine the L_2 norm and rank the POD eigenmodes to give a POD basis. The effects of using alternative variables for the L_2 norm have been discussed in Freund et al.[14]

Given a series of two-dimensional snapshots of the flow field, a matrix of dimension (M,N) is constructed:

$$\boldsymbol{X} = \left(x_{ji}\right) \tag{1}$$

where i corresponds to the ith snapshot, a vector representation of the two-dimensional spatial pressure field, and j corresponds to the jth element of snapshot i. N is the number of snapshots and M is the number of elements in each snapshot. Each column vector i of the matrix $\boldsymbol{X}$ can be expressed as:

$$\boldsymbol{X}_i = \begin{pmatrix} x_{1i} & x_{2i} & \cdots & x_{Mi} \end{pmatrix}^T \tag{2}$$

A mean field is constructed from all the snapshots:

$$\overline{\boldsymbol{X}} = \frac{1}{N}\sum_{i=1}^{N} \boldsymbol{X}_i \tag{3}$$

and a new zero mean data set is constructed:

$$\widetilde{\boldsymbol{X}}_i = \boldsymbol{X}_i - \overline{\boldsymbol{X}} \tag{4}$$

The auto-correlation matrix is formed by

$$\boldsymbol{C} = \widetilde{\boldsymbol{X}}^T \widetilde{\boldsymbol{X}} \tag{5}$$

and $\boldsymbol{C}$ is diagonalised using a singular value decomposition to give:

$$\boldsymbol{C} = \boldsymbol{V}\boldsymbol{\Lambda}\boldsymbol{V}^T \tag{6}$$

The trace of the diagonal matrix $\boldsymbol{\Lambda}$ gives the eigenvalues $\lambda_1 \geq \lambda_2 \geq \ldots \geq \lambda_N$ and $\boldsymbol{V}$ is the matrix of the associated eigenvectors. A POD basis matrix is constructed from the eigenvectors:

$$\boldsymbol{\Phi} = \widetilde{\boldsymbol{X}}\boldsymbol{V} \tag{7}$$

where

$$\boldsymbol{\Phi} = \left(\phi_{jk}\right) \tag{8}$$

constitutes the POD basis and $\boldsymbol{\Phi}_k$ corresponds to the kth POD basis vector:

$$\boldsymbol{\Phi}_k = \begin{pmatrix} \phi_{1k} & \phi_{2k} & \cdots & \phi_{Mk} \end{pmatrix}^T \tag{9}$$

A coefficient matrix is constructed from

$$\boldsymbol{A} = \boldsymbol{CV} \tag{10}$$

where

$$\boldsymbol{A} = \left(\alpha_{ik}\right) \tag{11}$$

where k corresponds to the kth POD mode and i corresponds to the ith snapshot coefficient of POD mode k. Each snapshot i can then be reconstructed by

$$\hat{\boldsymbol{X}}_i = \overline{\boldsymbol{X}} + \sum_{k=1}^{P} \alpha_{ik} \boldsymbol{\Phi}_k \tag{12}$$

If $P = N$ and N is the number of original snapshots, the data is reconstructed exactly. An approximation can be achieved, to an accuracy of Q%, by taking the first $P < N$ eigenvectors such that:[14]

$$\sum_{n=1}^{P} \lambda_n \Big/ \sum_{n=1}^{N} \lambda_n > \frac{Q}{100} \tag{13}$$

CAVITY FLOW RECONSTRUCTION

A POD basis has been constructed from 406 snapshots containing approximately 2.0 periods of the cavity flow history. Figure 2 shows the percentage of L_2 pressure contained within the first few eigenvalues, added-up according to Eq. 13. For the current study, a bounding value of $Q = 99.9\%$ was chosen. This is achieved by summing the first 9 eigenvalues. The cavity flow reconstruction over a complete period is given in Fig. 4. The POD time mean pressure field and the first 4 modes corresponding to the 4 most energetic eigenvalues are given in Figs. 5 (a-e). The coefficients associated with the first 4 modes are shown in Fig. 6. The reconstructed pressure fields in Fig. 4 are in excellent agreement with computed snapshots,[3] shown in Fig. 3, with the main features of the flow being distinctly captured. However, due to the truncation of the higher frequencies present within the flow, there is some smearing of the shock waves.

CAVITY FLOW EXTRAPOLATION

A method to extrapolate the cavity flow state beyond the original snapshots is presented. Figure 6 indicates that the time-dependent coefficients α_{ik} vary in a periodic form. These coefficients can be represented by a truncated discrete Fourier series to give an approximate set of coefficients $\tilde{\alpha}_{ik}$:

$$\tilde{\alpha}_{ik} = \sum_{l=1}^{R} \left(\chi_{k,l} + \beta_{k,l} \cos\left(\omega_{k,l} i\Delta t\right) + \delta_{k,l} \sin\left(\omega_{k,l} i\Delta t\right) \right) \tag{14}$$

where k denotes the number of the POD basis vector. l is the lth Fourier coefficient of mode k and R is the total number of Fourier modes. In this study, $R = 6$. Provided the flow is sufficiently stationary, Eq. 14 can be used to predict the time-dependent history of the coefficients beyond the original data-set time $N\Delta t$. This is obtained by substituting

$i > N$ into Eq. 14 to give $\tilde{\alpha}_{ik}$ at the later time $i\Delta t > N\Delta t$. The approximation $\tilde{\alpha}_{ik}$ is then placed in Eq. 12 replacing α_{ik} to obtain a projection $\hat{\boldsymbol{X}}_i$ of the pressure field at time $i\Delta t$.

ERROR ANALYSIS

To validate the POD extrapolation of the cavity flow, 18 periods of flow history generated with the numerical code have been used as a comparison, totalling 4147 snapshots of the flow field. Approximately 230 snapshots of the flow constitute 1 period T of flow oscillation.

The timeline defined by the 18 periods of flow history is subdivided into 3 sections of lengths $7T$, $10T$, and $1T$, as shown in Fig. 7. The first section of length $7T$ is used to construct the POD basis. This is based on s periods of flow history beginning at $t = (7-s)T$ and ending at $t = 7T$. In this study, $0 < s < 5.5$. The POD prediction begins at $t = 7T$ and continues to the end of the computed flow history. An error indicator to measure the accuracy of the prediction is introduced as the L_2 norm of the difference between the extrapolated and the computed pressure at the downstream edge (x=3.0D, y=0.0) constructed over the last period, $17T < t < 18T$:

$$e = \left(\frac{1}{T} \sum_{t=17T}^{18T} \left(p_{\Phi}(t) - p(t) \right)^2 \Delta t \right)^{1/2} \tag{15}$$

where $p_{\Phi}(t)$ is the pressure at the downstream edge at time t extrapolated from the POD basis, $p(t)$ is the pressure at the downstream edge that is computed by time-marching the CFD model to time t, and $\Delta t = T/230$.

As can be seen in Fig. 8, the error indicator is generally decreasing as the number of snapshots used to construct the POD basis increases. Interestingly, a larger error is obtained when an integer number of periods is used to construct the POD modes, while the minima occur at every odd half-period. This is verified by the extrapolations based on 2.5 and 3.0 periods of data. Pressure traces of these predictions are compared to pressure data obtained from advancing the CFD computation in time in Figs. 9 and 10. Figure 11 shows the pressure traces over the last period. It can clearly be seen that the POD prediction formed from the 2.5 periods of data (dashed line) overlaps the computed pressure trace (dotted line). The prediction using 3.0 periods of data (solid line) is less in agreement with the CFD benchmark. It is thought that the improved accuracy of the half-period basis is due to the algorithm being more successful at preventing sub-harmonic waveforms that may cause a 'beating' effect in the POD prediction.

CONCLUSIONS

A method has been presented for the prediction of cavity flow using a POD analysis. In the current study, the POD analysis reduces the information to a dataset of only 10 vectors, consisting of the mean field and 9 POD basis vectors. Although the generation of the basis is computationally expensive, the reconstruction of any snapshot requires a computational effort that is significantly lower than time-marching a CFD solution. The reconstructed flow field is in excellent agreement with the CFD computations. The

computational efficiency of the POD flow prediction has been further enhanced by reducing the coefficients matrix to a sum of Fourier series pairs from which the flow field is extrapolated in time. The pressure traces of the extrapolated flow field are also in excellent agreement with the CFD computations, with only minor degradation as the projected time increases. The reduction in computational effort required by a POD reconstruction to predict stationary cavity flow indicates that this method may be able to produce real-time projections. This promising feature suggests that the POD scheme may be able to be system-inverted to be used in a feed-back control loop for the cavity flow.

ACKNOWLEDGEMENTS

The support of EPSRC grant GR/N23745 is acknowledged. This work was performed using the University of Leicester Mathematical Modelling Centre's supercomputer that was purchased through the EPSRC strategic equipment initiative.

REFERENCES

[1]Charwat, A. F., Roos, J. N., Dewey, F. C. J., and Hitz, J, A., "An investigation of separated flow - Part I: The pressure field," *J. of the Aerospace Sciences*, **28**, pp. 457-470, June 1961.

[2]Zhang, X., "Compressible cavity flow oscillation due to shear layer instabilities and pressure feed-back," *AIAA Journal*, **33**, No. 8, pp. 1404-1411, Aug. 1995.

[3]Rona, A. and Brooksbank, E. J., "Injection parameters for an effective passive control of cavity flow instability," Paper 2002-0119, 40th AIAA Aerospace Sciences Meeting and Exhibit, Reno, NV, Jan. 2002.

[4]Heller, H. H., Holmes, D. G., and Covert, E. E., "Flow-induced pressure oscillations in shallow cavities," *J. Sound and Vibration*, **18**, No. 4, pp. 545-553, 1971.

[5]Heller, H. and Delfs, J., "Cavity pressure oscillations: The generating mechanism visualized," *J. Sound and Vibration*, **196**, No. 2, pp. 248-252, 1996.

[6]Grace, S., "An overview of computational aeroacoustic techniques applied to cavity noise prediction," Paper 2001-0510, 39th AIAA Aerospace Sciences Meeting and Exhibit, Reno, NV, Jan. 2001.

[7]Zhang, X., *An experimental and computational investigation into shear layer driven single and multiple cavity flowfields*, Ph.D. thesis, University of Cambridge, UK, 1988.

[8]Zhang, X. and Edwards, J. A., "Analysis of unsteady cavity flow employing an adaptive meshing algorithm," *Computers & Fluids*, **25**, No. 4, pp. 373-393, May 1996.

[9]Zhang, X., Rona, A., and Edwards, J., "An observation of pressure waves around a shallow cavity," *J. Sound and Vibration*, **214**, No. 4, pp. 771-778, July 1998.

[10]Lumley, J. L., "The structure of inhomogeneous turbulent flows," *Atm. Turb. and Radio Wave Prop.*, pp. 166-178, 1967.

[11]Rona, A. and Dieudonné, W., "Unsteady laminar and turbulent cavity flow models by second order upwind methods," Paper 99-0656, 37th AIAA Aerospace Sciences Meeting and Exhibit, Reno, NV, Jan. 1999.

[12]Kok, J., "Resolving the dependence on free-stream values for the k-omega turbulence model," *AIAA Journal*, **38**, No. 7, pp. 1292-1295, July 2000.

[13]Rona, A. and Bennett, W., "Non-uniform total temperature in a turbulent vortex street," Paper 2001-2467, 19th Applied Aerodynamics Conference, Anaheim, CA, Jun. 2001.

[14]Freund, J. B. and Colonius, T., "POD analysis of sound generation by a turbulent jet," Paper 2002-0072, 40th AIAA Aerospace Sciences Meeting and Exhibit, Reno, NV, Jan. 2002.

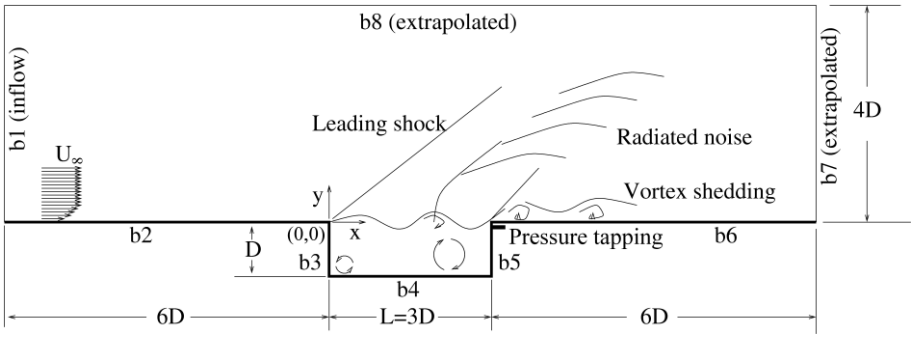

Fig. 1 Cavity geometry and computational domain

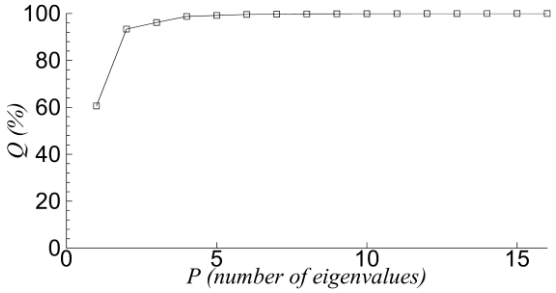

Fig. 2 Energy captured in the first P eigenvalues generated from a 2.0 period analysis.

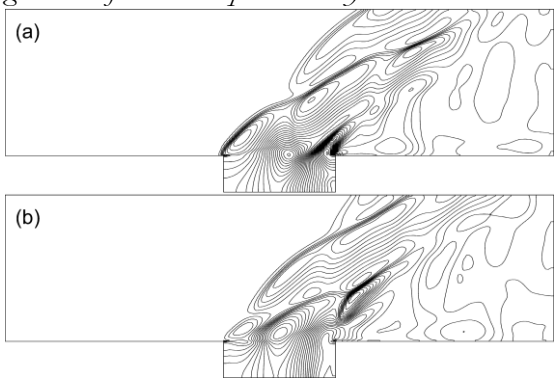

Fig. 3 Computed pressure contours over one time period T from Ref. 3: (a) t = 0.0, (b) t = 0.5T. $\Delta p = 0.003\,\rho_\infty U_\infty^2$.

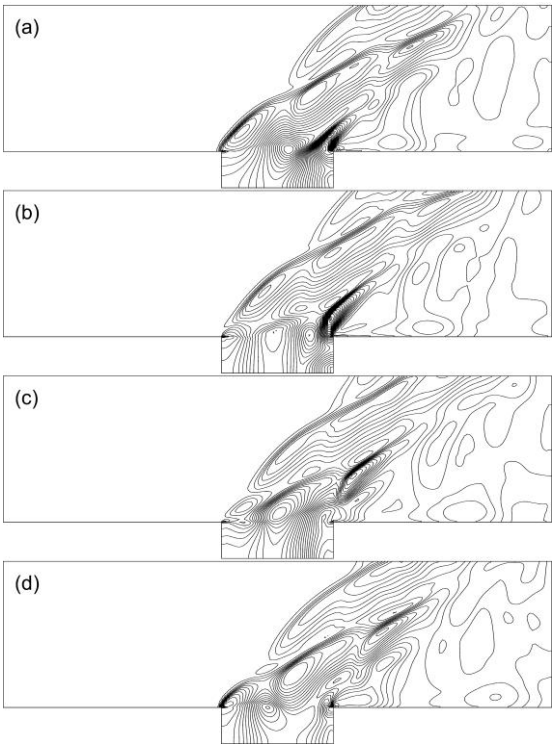

Fig. 4 Reconstructed pressure contours over one time period T, from 9 POD modes: (a) t = 0.0, (b) t = 0.025T, (c) t = 0.5T, (d) t = 0.75T. $\Delta p = 0.003\,\rho_\infty U_\infty^2$.

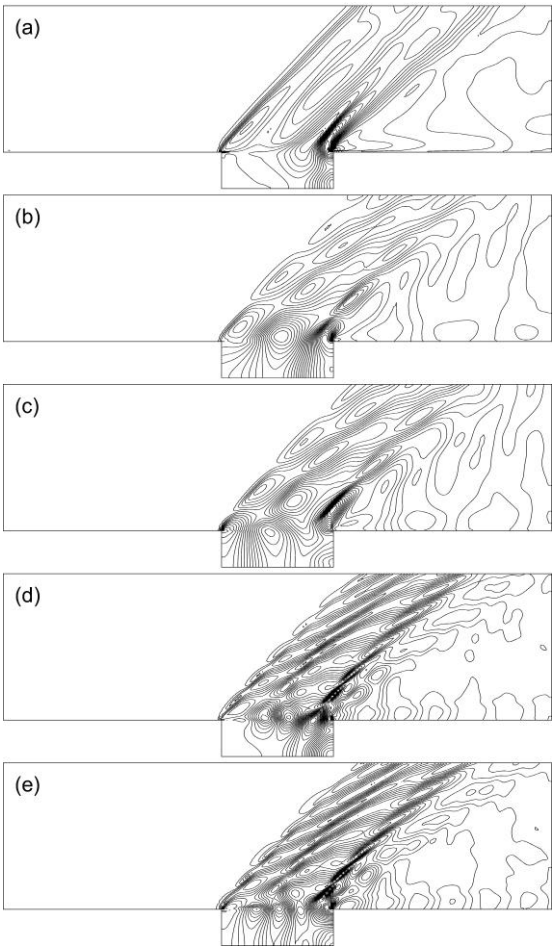

Fig. 5 POD modes: (a) mean pressure field, (b-e) the first 4 most energetic modes.

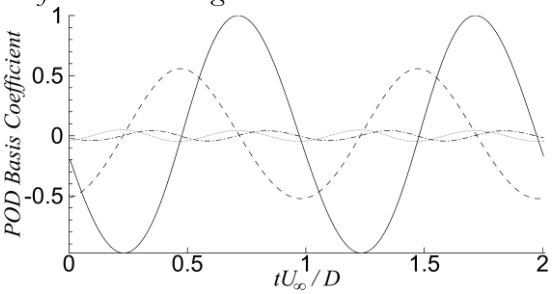

Fig. 6 Coefficients for the first 4 POD modes, generated from 2.0 periods of data, corresponding to Fig. 5: (—) b, (– –) c, (···) d, (–·–) e.

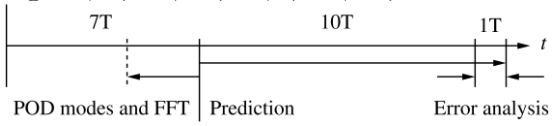

Fig. 7 Subdivision of the 18 period timeline.

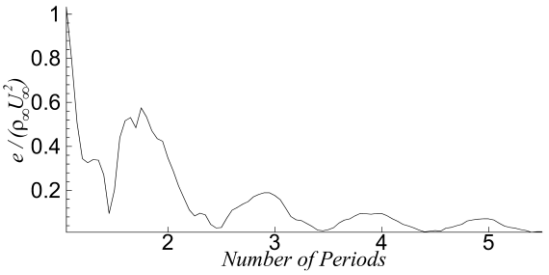

Fig. 8 Non-dimensional error over the last period.

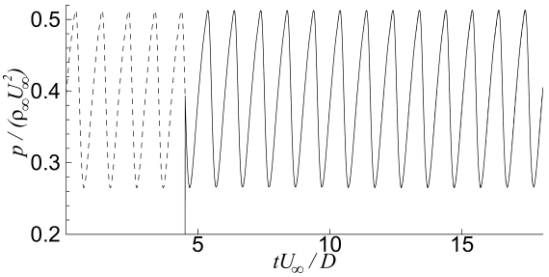

Fig. 9 Comparison of computed (– –) and extrapolated (—) pressure at downstream edge based on a POD basis generated from 2.5 periods of data.

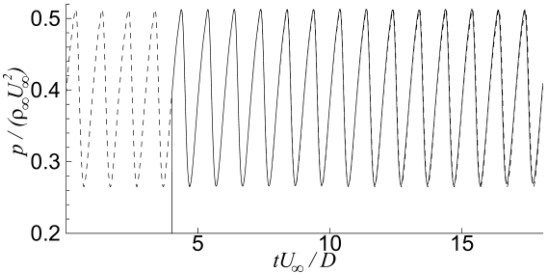

Fig. 10 Comparison of computed (– –) and extrapolated (—) pressure at downstream edge based on a POD basis generated from 3.0 periods of data.

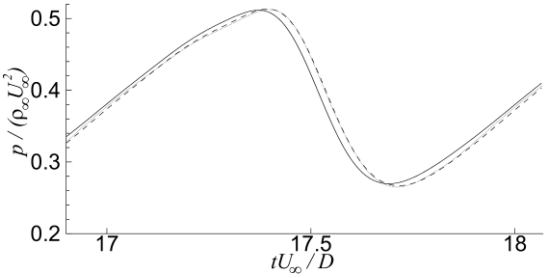

Fig. 11 Comparison of computed (···) and extrapolated pressure at downstream edge based on POD bases generated from 2.5 (– –) and 3.0 (—) periods of data. The dashed and the dotted lines overlap.